Nanotoxicology, March–December 2010; 4(1–4): 319–330

informa
healthcare

Impact of silver nanoparticles on human cells: Effect of particle size

WEI LIU[1], YUAN WU[1], CHANG WANG[1], HONG C. LI[1], THANH WANG[1], CHUN Y. LIAO[1,2], LIN CUI[1], QUN F. ZHOU[1], BING YAN[3,4], & GUI B. JIANG[1]

[1]*State Key Laboratory of Environmental Chemistry and Ecotoxicology, Research Center for Eco-Environmental Sciences, Chinese Academy of Sciences, Beijing,* [2]*Yantai Institute of Coastal Zone Research for Sustainable Development, Chinese Academy of Sciences, Yantai, Shandong,* [3]*School of Chemistry and Chemical Engineering, Shandong University, Jinan, China, and* [4]*St. Jude Children's Research Hospital, Memphis, Tennessee, USA*

(Received 3 August 2009; accepted 5 April 2010)

Abstract

This work investigated the cytotoxicities of three silver nanoparticles (SNPs) SNP-5, SNP-20 and SNP-50 with different sizes (~ 5 nm, ~ 20 nm and ~ 50 nm) using four human cell models (A549, SGC-7901, HepG2 and MCF-7). Endpoints included cell morphology, cell viability, cellular membrane integrity, oxidative stress and cell cycle progression. Observable deleterious effects on the cell morphologies and membrane integrity were induced by SNP-5 and SNP-20. SNPs elevated the ROS levels in cells and arrested the cells at S phase. Apoptosis occurred for 4–9% of the exposed cells. All these cellular responses as well as EC50 values were found to be size-dependent for the tested SNPs. Ultrastructural observations confirmed the presence of SNPs inside cells. Elemental analysis of silver in cells by ICP-MS showed that smaller nanoparticles enter cells more easily than larger ones, which may be the cause of higher toxic effects. The findings may assist in the design of SNP applications and provide insights into their toxicity.

Keywords: *Silver nanoparticles, cytotoxicity, size-dependent*

Introduction

Materials at nanometer scale exhibit remarkable characteristics such as extraordinary electric, light-emitting, and catalytic properties, and hold great promises in both industrial and biomedical applications (Service 2003). More and more products containing nanomaterials emerge in the commercial market and are present in our daily life. Of these various nanotechnology products, those containing silver nanoparticles (SNPs) belong to some of the fastest growing products, especially within the medical and healthcare sector. They are used as antimicrobial agents in wound dressings, surgical instruments, bone prostheses, room sprays, laundry detergents and wall paint. They can also be incorporated into textiles for the manufacture of clothing such as underwear and socks (Benn and Westerhoff 2008). All of these products usually come in direct contact with humans, which may increase the possibility of SNPs to enter human bodies, tissues and cells (Susan et al. 2009). Therefore, studies on the potential toxicities of SNPs are urgent for their biosafety evaluation due to their widespread application in various fields.

Bulk silver used to be considered as a non-hazardous element. Most of investigations about toxicities of silver focused on the elemental silver and silver ions (Ag^+). Based on available toxicological research, long-term exposure to silver ions could cause argyria, a permanent bluish gray pigmentation of the skin (Greene and Su 1987). Other toxic effects such as incidences of ventricular hypertrophy, hepatic necrosis and ultrastructural changes of the liver were also observed from exposure of 0.1% silver ions at a dose of 89 mg/kg/day in rats for 218 days (Olcott 1950). The release of free silver ions was demonstrated to be one mechanism of silver toxicities. The size of silver particles can influence the rate of release of silver ions. As preceding works revealed (Hussain et al. 2005; Hsin et al. 2008), the cytotoxicity of silver particles increases dramatically as their size reduced to nanoscale. It was reported that the toxic effects induced by SNPs (15 nm) were about

Correspondence: Gui Bin Jiang, State Key Laboratory of Environmental Chemistry and Ecotoxicology, Research Center for Eco-Environmental Sciences, Chinese Academy of Sciences, PO Box 2871, Beijing 100085, China. Tel: +86 10 62849179. Fax: +86 10 62849179. E-mail: gbjiang@rcees.ac.cn

ISSN 1743-5390 print/ISSN 1743-5404 online © 2010 Informa UK, Ltd.
DOI: 10.3109/17435390.2010.483745

50-fold more pronounced than those by silver carbonate (Braydich et al. 2005). Cytotoxicity of SNPs is likely attributed to the size of the particles because larger silver particles (250 μm) show no notable effects even at higher doses (Hsin et al. 2008). Compared to other metallic nanoparticles and micro-particles such as Fe_3O_4, Al, MnO_2, MoO_3 and W, SNPs at the sizes of 15 nm and 100 nm induce more significant toxicities to BRL 3A rat liver cells (Hussain et al. 2005). When used as a topical antimicrobial agent, SNPs with the diameter of 10 nm could destabilize the outer membrane, collapse the plasma membrane potential and deplete the levels of intracellular ATP in *Escherichia coli* cells. The antimicrobial action mode was similar to that of Ag^+ ions (Lok et al. 2006). While in algae cells, when compared as the function of the Ag^+ concentration, the toxicity induced by SNPs is much higher than that by $AgNO_3$ (Navarro et al. 2008). Although the use of SNPs is growing, there are still a number of important knowledge gaps about the safety of SNPs (Susan et al. 2009). Few studies discuss in detail the size-dependent cellular impacts, which may greatly limit the accurate biosafety assessment, as nanoparticles at various sizes possibly induce rather different effects on the organisms (Nel et al. 2006).

The present study investigated the multiple toxicities of SNPs on human cells and compared the impacts caused by SNPs at three different sizes. Associating with reports about the effect of silver ions and surface chemical modification, this work discussed the effect of particle size on the cytotoxicity of SNPs.

Materials and methods

Silver materials

The tested materials included three sizes of SNPs: SNP-5 (~ 5 nm), SNP-20 (~ 20 nm) and SNP-50 (~ 50 nm). SNP-5 and SNP-20 were purchased from Huzheng Nano Technology Limited Company (Shanghai, China). The protective agent of these commercial SNPs is the low toxic polyvinylpyrrolidone (PVP). SNP-50 was synthesized by reducing silver nitrate ($AgNO_3$) following a previously reported method with minor modification (Gu et al. 2002). Total 100 ml $AgNO_3$ solution (1 M) was dripped into 500 ml reducer aqueous solution which included 0.1 M sodium hypophosphite (NaH_2PO_2), 0.02 M H_2SO_4, 0.01 M sodium hexametaphosphate as disperser and 4.0 g PVP as protective agent. This reaction processed in 40–42°C bath water under constant magnetic stirring. The obtained silver colloid was centrifuged at 10,000 rpm for 15 min to remove the soluble chemicals involved in nanoparticle synthesis. Then 3 ml 1% passivant (1, 2, 3-benzitriazole) was added into the nanoparticles and removed after 20 min by centrifugation. Finally, the nanoparticles were rinsed with acetone and absolute ethanol and dried at 45°C for 24 h in a vacuum oven. The SNP-50 after dried was suspended in deionized water using sonication for 30 min in ice bath. The SNP-5 and SNP-20 were purified by the same wash process of SNP-50 before cell experiments. The final centrifugal supernatant of nanoparticle suspensions was used as solvent control.

The morphologies of SNPs were observed by transmission electron microscopy (TEM, Hitachi H-7500, Japan) and the particle sizes were identified by the nano particle size analyzer (N5, Backman, USA). Free Ag^+ in SNPs suspensions and cell culture medium was measured using a Silver Ion-Selective Electrode (Ag-ISE; JENCO, Shanghai, China).

All SNPs were suspended in deionized water to 1 g/l as stock suspensions by sonication. The stock suspensions of SNPs were maintained at 4°C in the dark and they can maintain monodispersed for several months. The exposure suspensions were prepared by series of dilution with cell culture medium by stirring for about 2 min just before each experiment. The silver nitrate solution was prepared in the same way as described above.

Design of the exposure experiments

The changes in cell viability and cell morphology were first studied in this study. $AgNO_3$, SNP-5, SNP-20 and SNP-50 were diluted to a series of concentrations (0.01, 0.1, 0.5, 1, 2.5, 5, 10, 25, 50 and 100 μg/ml) in cell culture medium to study the dose-related toxicities. Considering the discrepancy between different cell lines, four cell lines derived from different tissues (A549, HepG2, SGC7901 and MCF-7) were used to assure the universality of the toxicity effect. In the subsequent experiments, we chose HepG2 cells as the cell model. According to the EC50 values, series concentrations of $AgNO_3$ (0.01, 0.1, 1 μg/ml), SNP-5 (0.01, 0.1, 1 μg/ml), SNP-20 (0.1, 1, 10 μg/ml) and SNP-50 (0.1, 1, 10 μg/ml) were tested for their potential influences on membrane damage and oxidative stress of the cells. The cell cycle progression, apoptosis and necrosis in the cells treated with different doses (0.1, 0.5, 2.5 μg/ml) of $AgNO_3$, SNP-5, SNP-20 and SNP-50 were also investigated at time points of 6, 12 and 24 h. Negative control was performed in each experiment to confirm the feasibility of the cell lines.

Cell culture

The four types of commercial available cell lines used in this study were human lung adenocarcinoma ephithelial cells (A549), human stomach cancer cells (SGC-7901), human hepatocellular carcinoma cells (HepG2) and human breast adenocarcinoma cells (MCF-7). A549 and SGC-7901 were maintained in RPMI1640 medium (Hyclone, Logan, UT, USA). HepG2 and MCF-7 were cultured in Dulbecco's Modified Eagle's Medium (DMEM; Hyclone). All medium was supplemented with 10% fetal bovine serum (FBS; Gibco, Grand Island, NY, USA) and 100 U/ml penicilli/streptomycin (Gibco). All cell lines were grown at 37°C in a 5% CO_2 humidified environment. The cells at a logarithmic phase of growth were used for the exposure tests.

For assay of cell viability, cell morphology and intracellular ROS generation, cells were cultured in 96-well plates (Corning, Costar, NY, USA) at a density of 5000 cells per well with 150 µl culture medium. The measurement of membrane damage, SOD and GSH levels were performed in 35 × 10 mm dishes (Corning), and the density was 1×10^5 cells per dish with 2 ml culture medium. For analysis of internalization of silver nanoparticles, cell cycle progression, apoptosis and necrosis, cells were cultured in 100 × 20 mm dishes (Corning) at a density of 1×10^6 cells per dish with 10 ml culture medium. All cells were cultured for 24 h to achieve approximately 80% confluence before treated with various silver solutions.

Cell viability

The cell viability was examined using MTT assay (Mosmann 1983). Cells were exposed to $AgNO_3$, SNP-5, SNP-20 and SNP-50 for 24 h. At the end of exposure, 150 µl methyl- thiazoletetrazolium (MTT; Amresco, Solon, OH, USA) solutions (0.5 mg/ml in cell culture medium) were added to each well and the cells were incubated at 37°C for 4 h. After incubation, MTT solution was aspirated and the cells were treated with 150 µl dimethyl sulfoxide (DMSO; Amresco). The plates were slightly shaken at room temperature until the crystals dissolved. Absorbance was measured at 490 nm using a multimode microplate spectrophotometer (Thermo Electron, Varioskan Flash, USA).

Cell morphology

Changes of the cell morphology were observed using an optical microscope (Zeiss Axiovert 200, Jena, Germany). Hoechst 33342 staining was used to study alterations in the nuclear morphology. The exposed cells were washed with ice-cold phosphate-buffered saline (PBS, 0.1M) and treated with Hoechst 33342 (5 µg/ml; Amresco) in the dark at room temperature for 20 min, then observed by the fluorescent microscopy (Zeiss Axiovert 200) at the excitation wavelength of 365 nm.

Cellular uptake of silver nanoparticles

The tested chemicals $AgNO_3$, SNP-5, SNP-20 and SNP-50 were added at the exposure dose of 1 µg/ml. After 6 h, cells were collected and washed three times with PBS. An aliquot of the collected cells was digested with 300 µl HNO_3 and 100 µl 30% H_2O_2 for 12 h, then total silver concentration inside cells was measured in 5% HNO_3 solutions by ICP-MS (Agilent 7500, USA).

Another aliquot of the treated cells was used for TEM observation to further confirm the presence of silver nanoparticles inside the cells. The cells were washed three times with cold PBS, fixed in 2.5% glutaraldehyde for 12 h, then washed three times with PBS and post-fixed in 1% osmium tetroxide for 4 h. After fixation, specimens were washed three times with PBS, and dehydrated in a graded series of 50, 70 and 80% acetone and twice in 90%, for 10 min each, and twice in 100% acetone, for 15 min each. Samples were embedded in a mixture of EPON resin and polymerized at 60°C for 36 h. Ultra thin sections for TEM were prepared with a diamond knife, collected on copper grids, and contrasted with uranyl acetate and lead citrate. Samples were finally analyzed using TEM (Hitachi H-7500, Japan).

Cellular membrane integrity

The cellular membrane integrity was evaluated by lactate dehydrogenase (LDH) activity. 1% TWEEN 80 was used as the positive control and 0.1% PVP30 was used as solvent control. After 24 h exposure, the cell medium was collected and LDH activity in medium was determined using a commercial Kit (Jiancheng Bioengineering Institute, Nanjing, China).

Cellular oxidative stress

ROS generation, SOD and GSH levels were measured to indicate the cellular oxidative stress after exposure of silver nanoparticles. The ROS generation was determined by a fluorometric assay using intracellular oxidation of 2′, 7′-Dichlorofluorescin diacetate (DCFH-DA) after 2 and 24 h exposure. 10 µM

H_2O_2 was used as positive control (exposed for 0.5 h). The cells were washed with PBS and then incubated with 20 μM DCFH-DA for 30 min. At the end of DCFH-DA incubation, the cells were washed with PBS and lysed with DMSO. The aliquots were transferred to a black well plate (Corning). Then, the fluorescence of dichlorofluoroscein (DCF), as the oxidized product of DCFH-DA, was measured using the microplate spectrofluorometer (Thermo Electron) with excitation and emission wavelengths at 485 nm and 530 nm, respectively. For the visual image of ROS generation, the fluorescence in cells was visualized using the fluorescence microscope (Zeiss Axiovert 200) with an excitation wavelength of 485 nm.

For detection of SOD and GSH levels, the exposed cells were collected and lysed by cell lysates (Promega, Madison, WI, USA). SOD and GSH activities were measured by commercial kits (Jiancheng Bioengineering Institute, Nanjing, China). The measurements were carried out following the operation procedures in the specifications. An aliquot of the above cell lyses' samples was used to measure total protein concentration. The total protein was measured by the Bradford method (Bradford 1976) and bovine serum albumin (BSA) was used as standard.

Analysis of cell cycle progression

Cell cycle progression was analyzed using a flow cytometer (FACSCalibur, Becton Dickenson, CA, USA). After 24 h of exposure, the collected cells were washed by PBS and fixed using 70% ethanol for 2 h or longer. Ethanol was removed by centrifugation (1500 rpm, 5 min) and the cells were washed twice with PBS. Cells were then resuspended in PBS containing RNase (1 mg/ml; Sigma, St Louis, MO, USA) and propidium iodide (PI, 50 μg/ml; Sigma) and kept at 37°C in the dark for 30 min. The cell cycle was analyzed by measuring the amount of PI-labeled DNA in fixed cells by the flow cytometer.

Analysis of apoptosis and necrosis

Apoptotic and necrotic cell death were analyzed by double staining with Annexin V-FITC and PI, in which annexin V bound to the apoptotic and necrotic cells with exposed phosphatidylserine, while PI labeled the necrotic cells with membrane damage. 100 U/ml TNF-α (Calbiochem, San Diego, CA, USA) was used as positive control. After 24 h of exposure, the cells were collected and stained using Annexin V-FITC Apoptosis Detection Kit (Bender, Austria). Then, the samples were detected by the flow cytometer.

Statistics analysis

Results were expressed as the mean value ± standard deviation obtained from at least three independent experiments. Data were tested for statistical differences ($\alpha = 0.05$) using SAS system (SAS Institute Inc., Cary, NC, USA) by one-way analysis of variance (ANOVA) and Tukey-HSD method.

Results

Characterization of silver nanoparticles and their size-dependent cytotoxicity

The morphologies of SNPs observed by TEM are shown in Figure 1A–C. The particle sizes were 5.9 ± 3.3, 23.8 ± 6.7 and 47.5 ± 22.1 nm for SNP-5, SNP-20 and SNP-50, respectively (Figure 1D–F).

The free Ag^+ released by SNPs in cell culture medium was less than 1% under the conditions we used in the cytotoxicology experiments (see Supplementary Figure S1 B, online version only).

Based on MTT assay, the dose-dependent toxicity of SNPs was measured in A549, HepG2, MCF-7 and SGC-7901 cells. Comparison of EC50 values based on both mass concentration (Table I) and surface area (Table II) showed that the SNP with the smallest size (SNP-5) was the most toxic material to cells. In Table I, the order of toxicity was as follows: SNP-5 > Ag^+ > SNP-20 > SNP-50 for all four cell lines, indicating that the toxicity was negatively correlated with the nanoparticle sizes.

Cell morphological changes

Morphological observations indicated dose-related alterations in the exposed HepG2 cells. Cells in the negative control group showed normal shuttle shapes and they grew by adhering to the wall of culture plate. After 24 h of exposure to 1 μg/ml $AgNO_3$, the cells became round and detached from the culture plate. The cells in the 1 μg/ml SNP-5 exposure group became swollen. For SNP-20 and SNP-50 (both at 10 μg/ml) exposure groups, some of cells maintained normal structures, while the others appeared collapse.

The Hoechst 33342 staining is a common method to analyze the nuclear morphology of cells (Allen et al. 2001). Under fluorescent microscope, the negative control cells were stained uniformly blue (Figure 2A). In groups treated with $AgNO_3$ and SNP-5 (both at

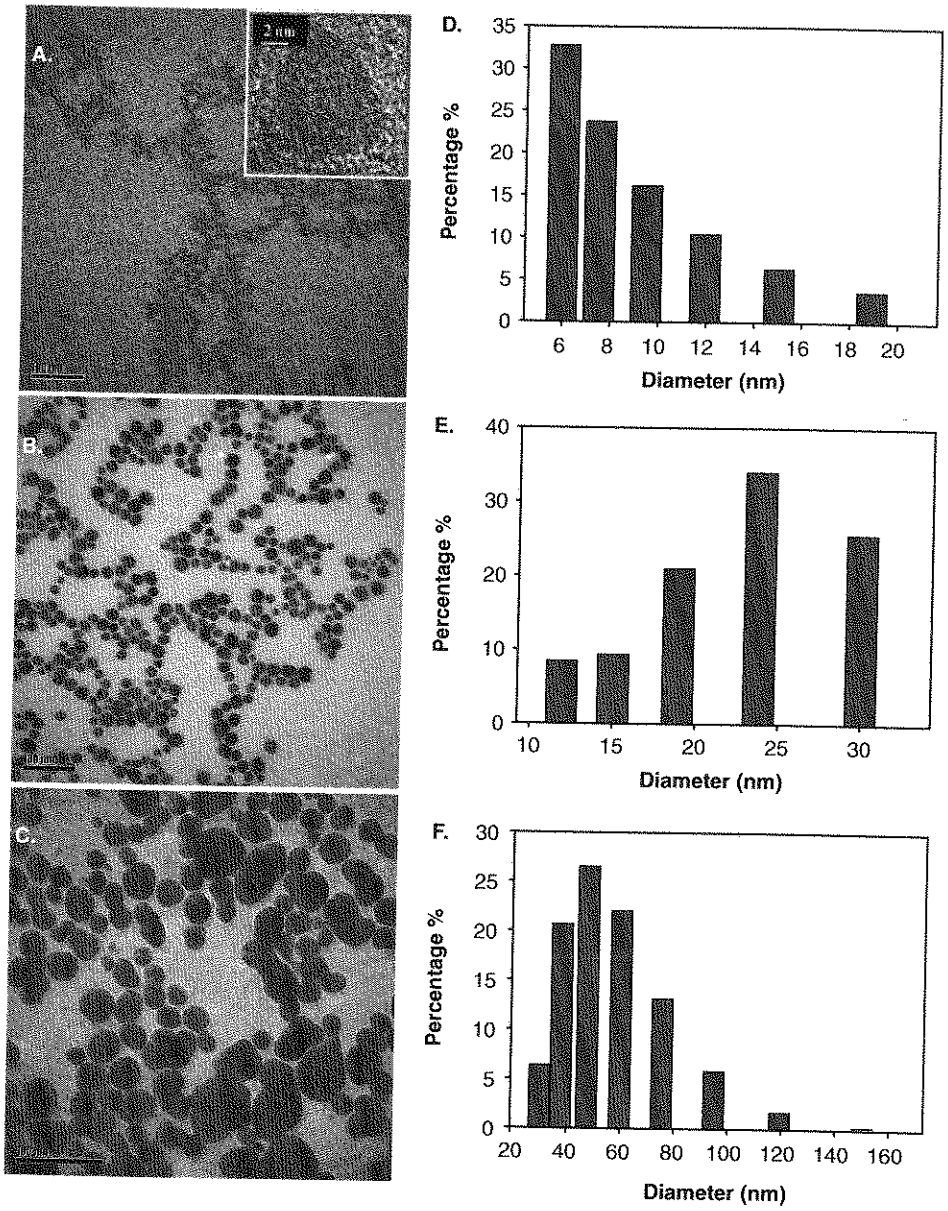

Figure 1. Transmission electron microscopy (TEM) images of silver nanoparticles. (A) SNP-5, inset shows a high resolution transmission electron microscopy (HRTEM) image of SNP-5; (B) SNP-20; (C) SNP-50. The scale is 100 nm. (D–F) The size distribution of SNP-5 (D), SNP-20 (E) and SNP-50 (F) (see colour version of this figure in the online version of this article).

Table I. Median effective concentration (EC50) for cell mortality in four different cell lines after exposure to Ag^+, SNP-5, SNP-20, SNP-50 for 24 hours.*

Cell lines	$AgNO_3$ (μg/ml)	SNP-5 (μg/ml)	SNP-20 (μg/ml)	SNP-50 (μg/ml)
A549	3.62 ± 0.96	1.02 ± 0.05	9.96 ± 1.84	14.31 ± 2.08
HepG2	1.11 ± 0.27	0.59 ± 0.14	25.35 ± 4.65	33.57 ± 10.52
MCF-7	1.81 ± 0.81	0.51 ± 0.02	14.33 ± 5.61	47.64 ± 14.67
SGC-7901	3.23 ± 0.48	0.92 ± 0.07	50.94 ± 3.85	112.03 ± 41.89

*EC_{50} was regressed by the four parameter logistic curve (Sigma Plot 10.0): $y = min + [(max - min)/1 + (x/EC50)^{Hillslope}]$. Standard deviation was calculated by four replications.

Table II. Values of EC50 based on specific surface area of silver nanoparticles.

Cell lines	SNP-5 (m^2/ml)	SNP-20 (m^2/ml)	SNP-50 (m^2/ml)
A549	0.12 ± 0.01	0.28 ± 0.05	0.16 ± 0.02
HepG2	0.07 ± 0.02	0.72 ± 0.13	0.38 ± 0.12
MCF-7	0.06 ± 0.00	0.41 ± 0.16	0.54 ± 0.17
SGC-7901	0.10 ± 0.01	1.46 ± 0.09	1.28 ± 0.48

1 μg/ml), a majority of cell nucleus were condensed as bright dots (Figure 2B and 2C, marked by open arrows). There were also some nuclear fragments (several small dots inside one single cell, marked by arrowheads) and apoptotic bodies (small dots alongside of big ones, marked by thick arrows). In SNP-20 and SNP-50 treated groups (both at 50 μg/ml, Figure 2D and 2E), most cells were normal and stained uniformly blue. Only a few cases of nuclear condensation, nuclear fragments and apoptotic bodies were observed.

Cellular uptake of silver nanoparticles

The cellular uptake of different sizes of silver was studied to elucidate the possible mechanism of the cytotoxicity of SNPs. The cellular uptake was detected after 6 h exposure. Washing the cells three times can remove some of SNPs on the cellular membrane, but membrane-bound SNPs may not be completely excluded. Measurement of total silver concentration in cells showed that 0.004–0.031% of silver entered into the cells. Relatively higher levels of silver were present in cells exposed to SNP-5 than to SNP-20 and SNP-50 (Figure 3), indicating the potential size-dependent cellular uptake of SNPs. In addition, the cellular silver levels in cells cultured in fetal bovine serum (FBS)-free medium increased by 33.8 ± 8.78% as compared to those in 10% FBS-containing medium (Figure 3). This observation might be due to binding of SNPs with proteins in FBS, which decreases the amount of available SNPs to enter the cells. TEM image was obtained to further confirm the cell-uptake of SNPs. Compared with the untreated cells (Figure 4A), there were many clumps of SNPs in endosomes and cytoplasm in SNP-treated cells (Figure 4B–D, indicated by black thick arrows).

Cell membrane integrity

As the released LDH is proportional to the number of cells with membrane damage (Haslam et al. 2000), extracellular LDH levels were investigated to evaluate the cell membrane damage elicited by SNPs. The solvent control showed no impact on the cell membrane integrity, means the effect was caused by silver materials alone. A dose-related increase in the extracellular LDH levels was found in all exposure groups after 24 h (Figure 5), which suggested that the exposed cell membranes were damaged, leading to the leakage of intracellular LDH. The ability of eliciting LDH leakage was in the order of $AgNO_3$ > SNP-5 > SNP-20 > SNP-50, which was similar to the trend for cell viabilities.

Cellular oxidative stress

Oxidative stress in cells can be evoked by the cellular uptake behavior of extraneous particles or by the redox and catalytic properties of the internalized particles (Lynch et al. 2006; Limbach et al. 2007; Auffan et al. 2008). To investigate the cellular oxidative stress induced by SNPs, we measured the changes in intracellular reactive oxygen species (ROS) generation, SOD activity and GSH levels. From the fluorescence images (Figure 6B), the brightest green fluorescent cells were from the positive control group, confirming the feasibility of the method for ROS evaluation. After 2 h of exposure, the fluorescent intensity was enhanced. This effect could still be observed after 24 h. Compared to the negative control group (Figure 6A), relatively strong fluorescent cells were observed in those treated with $AgNO_3$ (1 μg/ml) and SNPs (1 μg/ml) (Figure 6C–F), indicating that ROS were evoked by $AgNO_3$ and SNPs. Quantitative analysis of intracellular ROS levels showed that the relative fluorescent intensities increased to 241.36 ± 61.01%, 238.18 ± 12.00%, 165.43 ± 19.35%, and 147.48 ± 13.91% of the negative control in $AgNO_3$ (1 μg/ml), SNP-5 (1 μg/ml), SNP-20 (10 μg/ml), and SNP-50 (10 μg/ml) groups after 24 h exposure (Figure 6G). It is lower than that of 2 h of exposure (Figure 6H). SNPs also caused depletion of SOD activity and disturbance of GSH levels in a dose-dependent manner (Figure 7A, 7B). Results suggested that internalization of SNPs disturbed the cellular antioxidant defense system by

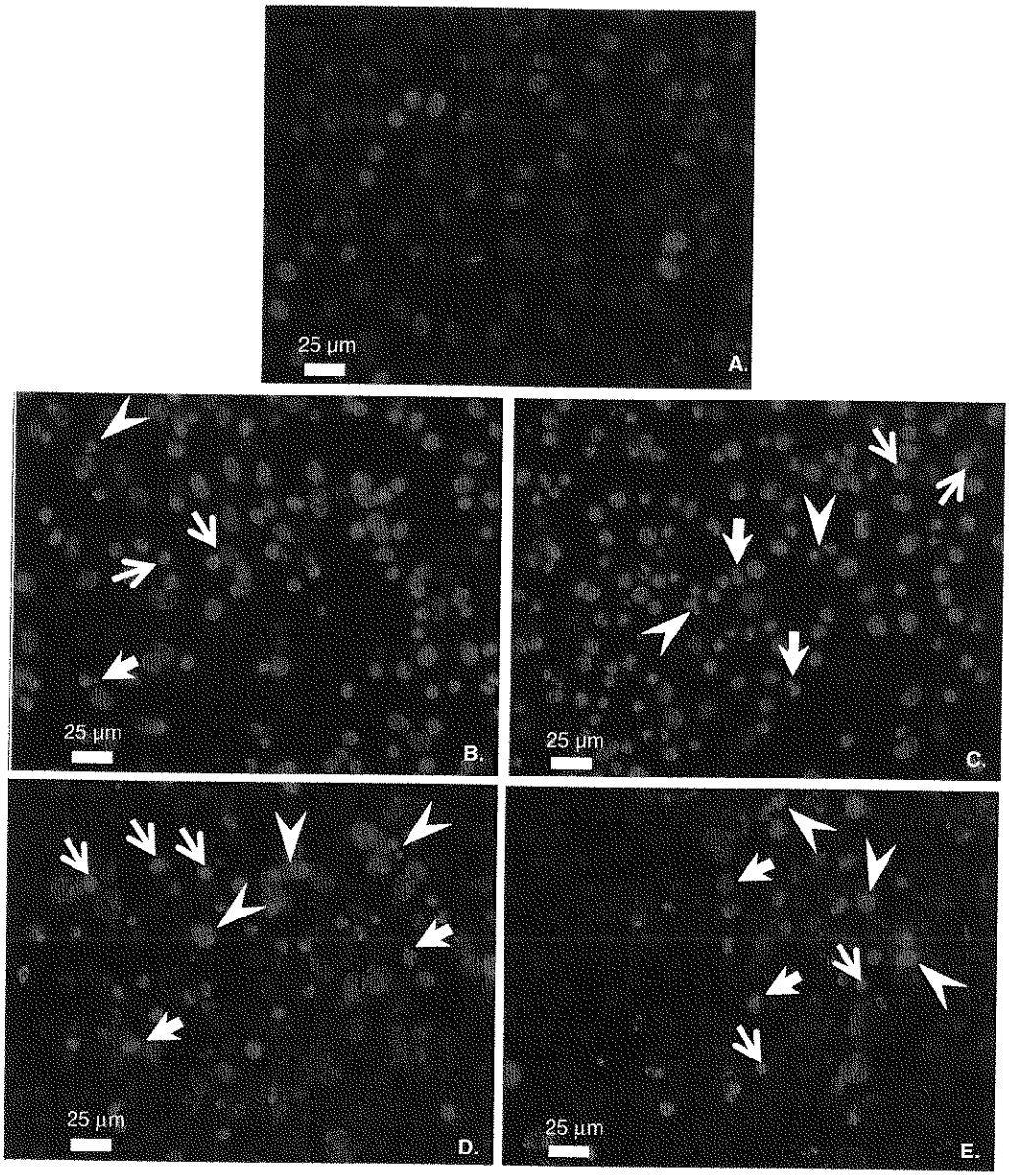

Figure 2. Micrographs of Hoechst 33342 stained cellular nuclear of HepG2 cell line. Images obtained at ×200 magnification. (A) Negative control; (B) $AgNO_3$ 1 µg/ml; (C) SNP-5 1 µg/ml; (D) SNP-20 50 µg/ml; (E) SNP-50 50 µg/ml. (Open arrows: nuclear condensation; Arrowheads: nuclear fragments; Thick arrows: apoptosis bodies) (see colour version of this figure in the online version of this article).

evoking ROS, exhausting the antioxidant enzymes, and changing the levels of the antioxidant molecules.

Cell cycle progression

The cellular oxidative stress may affect the cell cycle progression by producing early DNA damage. There are four distinct phases in a population of proliferating cells: growth and preparation of the chromosomes for replication (G1 phase), synthesis of DNA and duplication of the centrosome (S phase), preparation for mitosis (G2 phase) and mitosis (M phase) (Nunez 2001). To study the influences of SNPs on the cell cycle progression, the exposed cells were measured by flow cytometry after propidium iodide (PI) staining. As shown in Figure 8A, after 24 h exposure, the relative amounts of G1 phase decreased from 75.53 ± 0.79% to 68.06 ± 2.85%, 64.82 ± 5.36%, 69.93 ± 2.30% and 73.77 ± 1.22% for $AgNO_3$, SNP-5, SNP-20 and SNP-50 (all at 0.5 µg/ml, 24 h), respectively, whereas those in S phase increased from 17.85 ± 0.21% to 24.15 ± 2.23%, 27.54 ± 4.85%, 22.27 ± 1.85% and 19.88 ± 1.20%. These changes in G1 and S phase suggested that cell cycle events were disturbed by SNPs. The order of the cell cycle arrest was SNP-5 > Ag+ > SNP-20 > SNP-50.

Apoptosis and necrosis

It is known that irreparable DNA damage will eventually lead to cellular apoptosis. During apoptosis, the cellular chromosome DNA loses small DNA fragments, which can be determined by flow cytometry as the hyplo-diploid cell in subG1 phase. In this study, the ratio of subG1 cells in control cells was 1.27%, while it respectively increased to 8.08%, 12.85%, 5.42% and 5.26% in $AgNO_3$ (2.5 μg/ml, 6 h), SNP-5 (2.5 μg/ml, 6 h), SNP-20 (2.5 μg/ml, 24 h) and SNP-50 (2.5 μg/ml, 24 h) exposure groups without obvious subG1 peaks in the cellular DNA content histograms (the data was shown in Supplementary Table SI, online version only).

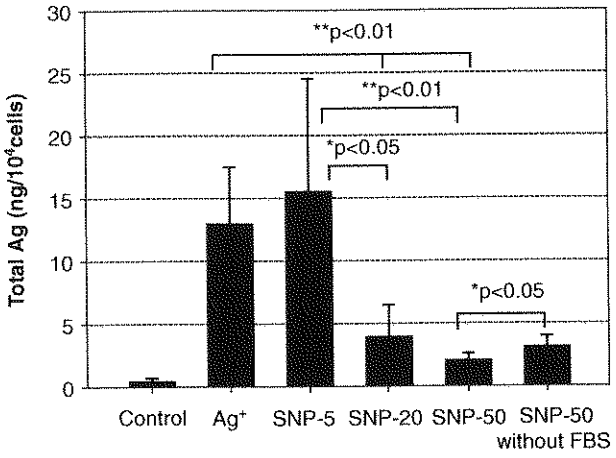

Figure 3. Total silver concentrations in HepG2 cells after exposure to $AgNO_3$, SNP-5, SNP-20 and SNP-50 (1 μg/ml) for 6 hours.

The relative amount of apoptosis cells (sum of the early apoptosis cells and the late apoptosis cells) were 4.64 ± 0.68%, 8.28 ± 1.88%, 6.53 ± 1.16% and 4.58 ± 2.44% for $AgNO_3$, SNP-5, SNP-20 and SNP-50 (all at 0.5 μg/ml, 24 h), with the control group at 2.39 ± 0.33%. Despite the increased fraction of apoptotic cells in the silver exposed groups, there was no significant difference between the treated and control groups for necrosis (Figure 8B), implying that the SNP-induced cell death is mainly caused by apoptosis.

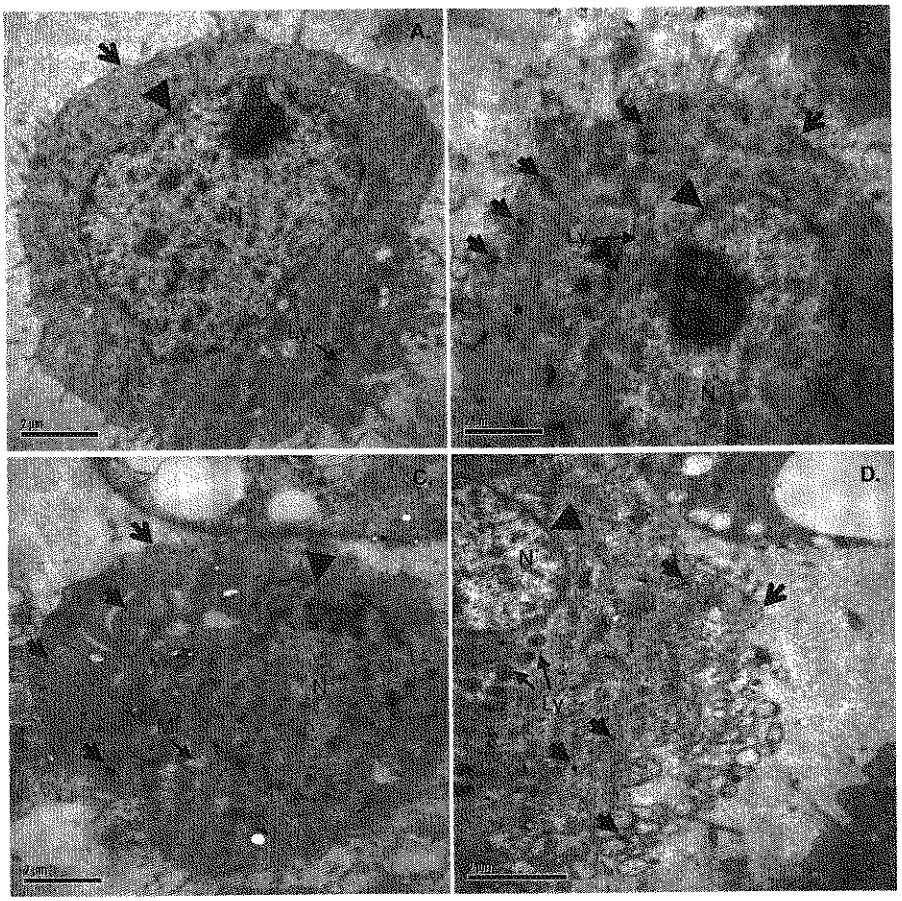

Figure 4. TEM images of SNPs internalization in HepG2 cells after exposure at 1 μg/ml for 6 hours. (A) Untreated control; (B) SNP-5; (C) SNP-20; (D) SNP-50. Black thick arrows: silver nanoparticles. Arrow heads: membrane of nucleus. Open arrows: membrane of cells. N: nuclear of cell; Mi: mitochondria; Ly: lysosome. The scale is 2 μm.

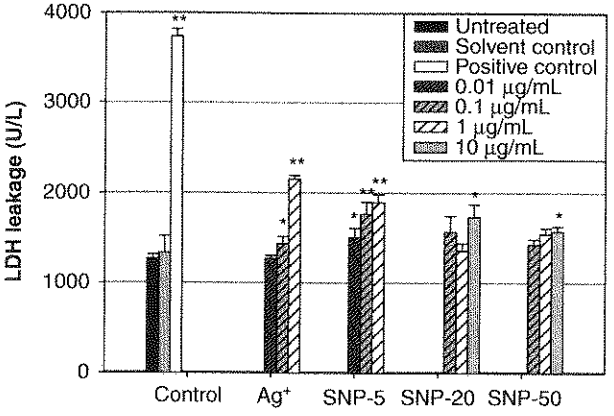

Figure 5. The LDH levels in cell medium after the HepG2 cells were treated with $AgNO_3$, SNP-5, SNP-20 and SNP-50 for 24 hours. $^*p < 0.05$, $^{**}p < 0.01$.

Discussion

There is a long history of using silver and silver compounds in antibacterial products. Silver at nanoscale was reported to possess stronger antibacterial activities than silver ions and have similar mode of action (Lok et al. 2006; Choi and Hu 2008). However, there is no comprehensive study currently which compares the cytotoxicity of silver ions and SNPs in human cells. Considering their potential applications in daily life, SNPs may enter human body through various routes such as the respiratory tract, gastrointestinal tract, skin and blood (Takenaka et al. 2001; Gan et al. 2004; Trop et al. 2006; Zhang and Sun 2007). Recent research has indicated that various tissues such as lung and liver might be important

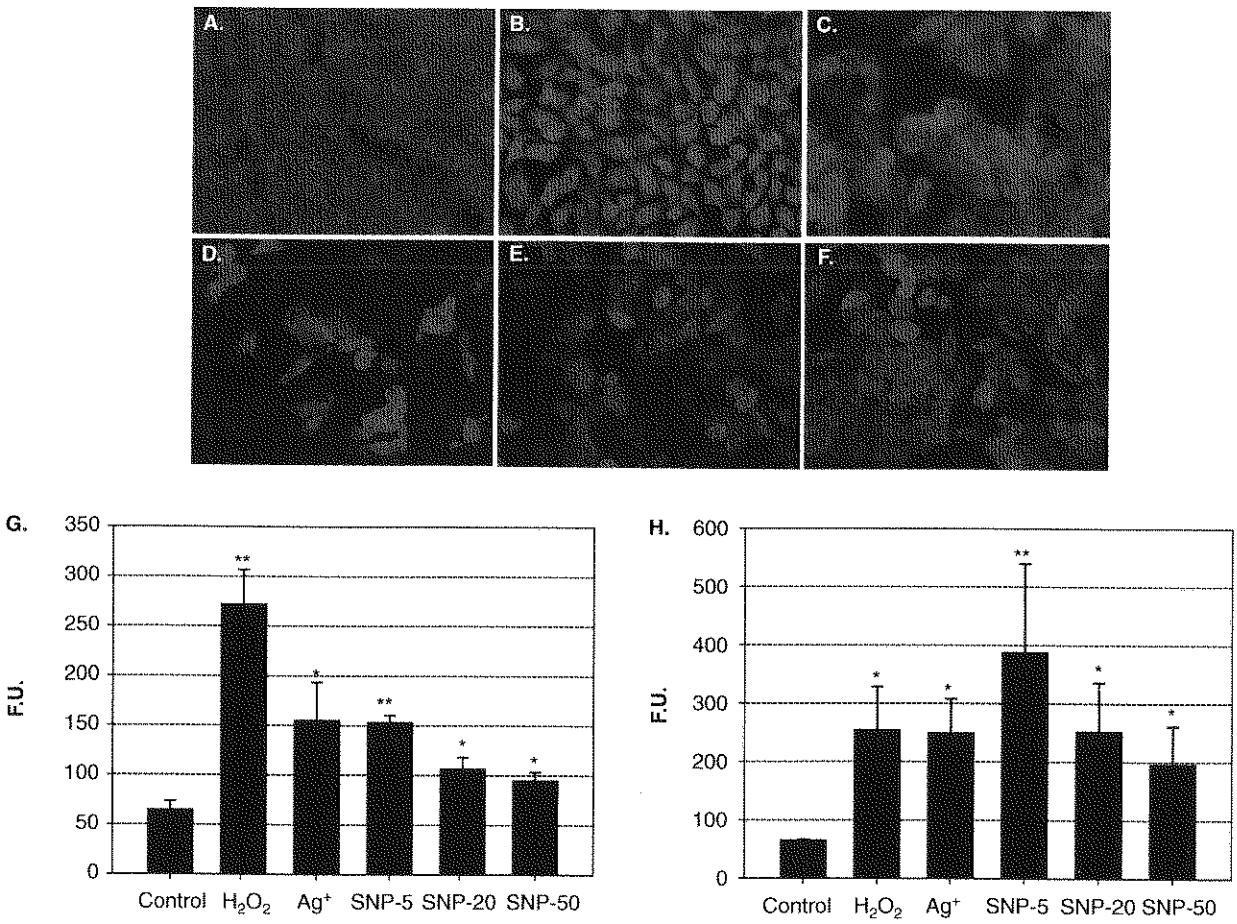

Figure 6. Intracellular ROS levels in HepG2 cells. (A–F) Fluorescence images. Images obtained at ×200 magnification. (A) Negative control; (B) Positive control (10 μM H_2O_2); (C) $AgNO_3$ (1 μg/ml); (D) SNP-5 (1 μg/ml); (E) SNP-20 (10 μg/ml); (F) SNP-50 (10 μg/ml). (G) The relative fluorescent intensity in cells after exposure for 24 h; (H) The relative fluorescent intensity in cells after exposure for 2 h. $^*p < 0.05$, $^{**}p < 0.01$ (see colour version of this figure in the online version of this article).

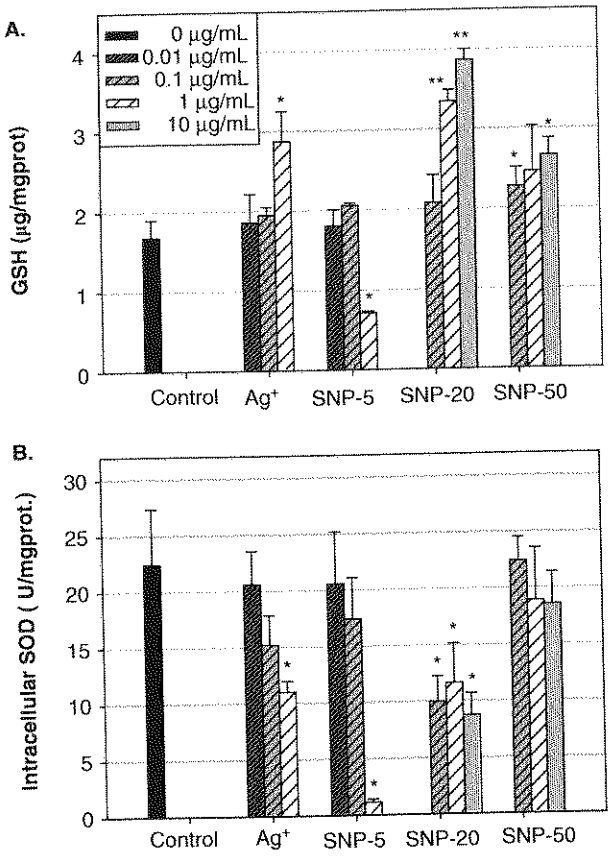

Figure 7. The intracellular GSH (A) and SOD (B) levels after HepG2 cell exposed to $AgNO_3$ and SNPs for 24 hours. $*p < 0.05$, $**p < 0.01$.

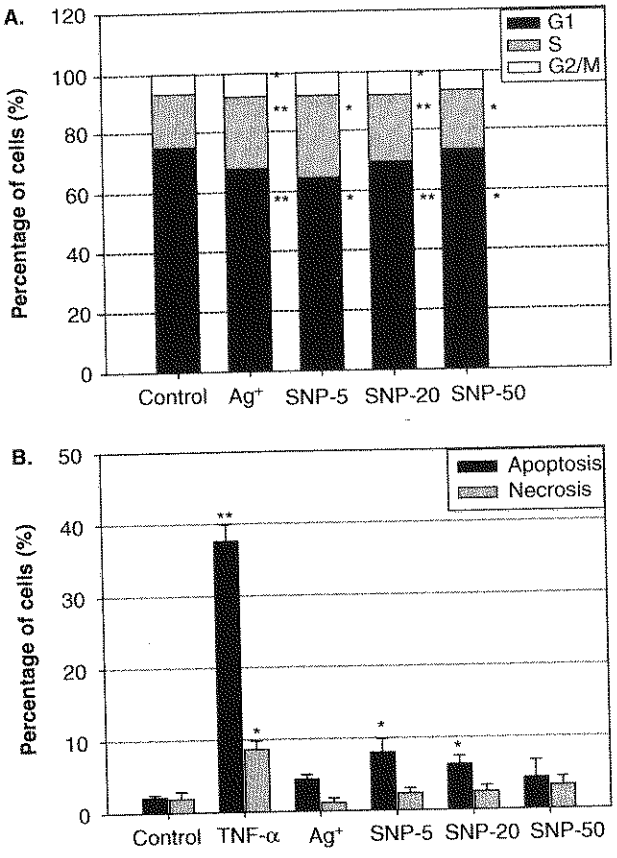

Figure 8. The cell cycle changes (A) and apoptosis/necrosis (B) induced by SNPs treatment (0.5 μg/ml, 24 hours) in HepG2 cells. $*p < 0.05$, $**p < 0.01$.

targets for SNPs (Susan et al. 2009). Four cell lines which are derived from different human organs were thus selected to evaluate the *in vitro* effects of SNPs in the present study. SNPs at three different sizes exhibited apparent toxicity to all the tested cell lines. In order to ensure the comparability of the two SNPs bought from a commercial supplier with the third SNP synthesized in-house, the same protective agent was used and special washing, processing and purification steps were carried out. Furthermore, the final centrifugal supernatant was used as a solvent control in the cell experiments. The cytotoxicity of SNPs is presented in mass concentration (Table I) and surface area (Table II). SNP-5 showed the highest toxicity with even less surface areas indicating that other behavior of SNP-5 such as cellular interactions might make extra negative contributions.

The internalization of SNPs at various sizes was observed in the exposed cells. SNPs might firstly disturb cellular membrane integrity in the process of entering cells. In previous studies, cell membrane damage was considered to be the mechanism for the cytotoxicity of Ag^+ (Chen and Schluesener 2008). It was attributed to the binding between Ag^+ and thiol groups in proteins that on the cellular membrane. In the cell culture medium, the Ag^+ released by SNPs was lower than 1% for three kinds of SNPs. The released Ag^+ may be one factor that contributes to the toxicity of SNPs. On the other hand, Navarro et al. (2008) observed Ag^+ on the surface of SNPs and suggested that the SNPs might interact with proteins and enzymes with thiol groups through the surface silver ions. As earlier research reported, the descent of a particle size allows a greater proportion of its atoms to be displayed on the surface rather than the interior of the particle (Oberdörster et al. 2005). Hence we speculate that the SNP-5 in this study possesses of the strongest activity to interact with the cellular membrane. Our results confirmed that SNP-5 led to the most serious damage to the cellular membrane compared to SNP-20 and SNP-50 at the same dose (1 μg/ml; Figure 3).

The potential toxicity mechanism of SNPs could also be related to their catalytic properties (Shen et al. 2004; Limbach et al. 2007). At nanoscale, both the surface atoms and structural defects increase

exponentially as the particle size decrease, as well as the active sites on the particle surface (Nel et al. 2006). In view of the large specific surface area, various nanoparticles have been found to churn out a plethora of ROS and provoke oxidative stress (Kaewamatawong et al. 2006). A boost of intracellular ROS was also observed in this study, suggesting that SNPs could lead to oxidative stress in cells, which was further validated by the changes in SOD activities and GSH levels. The ROS-generating capability of SNPs was also inversely proportional to the particle size (Figure 6G). Under normal condition or mild stress, ROS can be easily neutralized by antioxidant enzymes (such as SOD or GSH). However, under violent stress, ROS generation may be overwhelming and antioxidant enzymes and molecules may be exhausted. In this study, all of SNP-5, SNP-20 and SNP-50 could induce a drop of SOD activity but only SNP-5 depleted the GSH level. The stronger oxidative activity of SNP-5 is probably dues to two facts: The more catalytically active sites and the easier internalization in cells (Figure 5). Both facts have a direct relationship with the particle size.

Oxidative damage usually results in interference of cell cycles. As observed herein, the exposure of SNPs disturbed the cell cycle progression and caused a decrease of cells in the G1 phase and cell cycle arrest in S phase (Figure 8A). The G1 phase is important in the cell cycle because cells grow and prepare chromosomes for replication during this stage. The S phase arrest will allow cells to repair the DNA damage prior to mitosis. If the damage is severe and irreparable or if the repair pathway fails, cells will undergo apoptosis or necrosis. Previous studies showed conflicting results regarding to SNP-induced apoptosis (Arora et al. 2008; Asharani et al. 2009). In this study, apoptotic bodies in Hoechst stained cells and those in subG1 phase were observed after SNPs treatments (Figure 2), but the annexin V/PI staining data showed that the proportion of apoptotic cells was lower than 10% (Figure 8B). The result was consistent with the report in AshaRani's work (AshaRani et al. 2009). No massive apoptosis could be attributable to the result of damage repair process during cell cycles. Further studies are still necessary to explain the mechanism of cell death induced by SNPs.

In sum, the toxicological activities of SNPs were found to be size-dependent based on the assessment of the tested endpoints. SNP-5 exhibited the highest activity in cell morphological changes, cell membrane damage, ROS generation, and cell cycle arrest and cell apoptosis, even more toxic than silver ions in cell cycle arrest and cell apoptosis. Results also showed that SNP-5 could enter into cells much easier compared to SNP-20 and SNP-50. Similar results were also observed for other nanoparticles such as TiO_2 and gold nanoparticles (Chithrani and Chan 2007; Pan et al. 2007; Wang et al. 2007, Nan et al. 2008). The corresponding biological reactivity of smaller particles is expected to be higher, and may lead to higher toxicity. The results from this study are in line with previous studies on the size-dependent toxicity of gold nanoparticles and SNPs to microorganisms (Pan et al. 2007; Choi and Hu 2008). These findings provided insights into the size-dependent toxicities of SNPs in human cells, which implied the risk of nanoparticles with smaller size. *In vivo* studies will be conducted to achieve more objective assessment on the risk of SNPs.

Declaration of interest: We are grateful to National Natural Science Foundation of China (20537020), Chinese Academy of Sciences (KZCXZ-YW-420-21) and Key Project in the National Science & Technology Pillar Program (2007BAC27B02-1a) for the financial support. The authors would like to report no conflict of interests. The authors are entirely responsible for the content and writing of the manuscript.

References

Allen S, Sotos J, Sylte MJ, Czuprynski CJ. 2001. Use of Hoechst 33342 staining to detect apoptotic changes in bovine mononuclear phagocytes infected with Mycobacterium avium subsp paratuberculosis. Clin DiagnLab Immunol 8:460–464.

Arora S, Jain J, Rajwade JM, Paknikar KM. 2008. Cellular responses induced by silver nanoparticles: In vitro studies. Toxicol Lett 179:93–100.

Asharani PV, Mun GLK, Hande MP, Valiyaveettil S. 2009. Cytotoxicity and genotoxicity of silver nanoparticles in human cells. ACSnano 3:279–290.

Auffan MAW, Rose J, Roncato MA, Chaneac C, Waite DT, Masion A, Woicik JC, Wiesner MR, Bottero JY. 2008. Relation between the redox state of iron-based nanoparticles and their cytotoxicity toward Escherichia coli. Environ Sci Technol 42:6730–6735.

Benn TM, Westerhoff P. 2008. Nanoparticle silver released into water from commercially available sock fabrics. Environ Sci Technol 42:4133–4139.

Bradford MM. 1976. Rapid and sensitive method for quantitation of microgram quantities of protein utilizing principle of protein-dye binding. Anal Biochem 72:248–254.

Braydich SL, Hussain S, Schlager JJ, Hofmann MC. 2005. In vitro cytotoxicity of nanoparticles in mammalian germline stem cells. Toxicol Sci 88:412–419.

Chen X, Schluesener HJ. 2008. Nanosilver: A nanoproduct in medical application. Toxicol Lett 176:1–12.

Chithrani BD, Chan WCW. 2007. Elucidating the mechanism of cellular uptake and removal of protein-coated gold nanoparticles of different sizes and shapes. Nano Lett 7: 1542–1550.

Choi O, Hu ZQ. 2008. Size dependent and reactive oxygen species related nanosilver toxicity to nitrifying bacteria. Environ Sci Technol 42:4583–4588.

Gan X, Liu T, Zhong J, Liu X, Li G. 2004. Effect of silver nanoparticles on the electron transfer reactivity and the catalytic activity of myoglobin. Chembiochemistry 5:1686-1691.

Greene RM, Su WPD. 1987. Argyria. Am Fam Phys 36:151–154.

Gu DM, Gao N, Cheng JN. 2002. High-speed preparation of nanometer silver by reduction with sodium hypophosphite in liquid phase. Final Chem 19:634–636.

Haslam G, Wyatt D, Kitos PA. 2000. Estimating the number of viable animal cells in multi-well cultures based on their lactate dehydrogenase activities. Cytotechnology 32:63–75.

Hsin YH, Chena CF, Huang S, Shih TS, Lai PS, Chueh PJ. 2008. The apoptotic effect of nanosilver is mediated by a ROS- and JNK-dependent mechanism involving the mitochondrial pathway in NIH3T3 cells. Toxicol Lett 179:130–139.

Hussain SM, Hess KL, Gearhart JM, Geiss KT, Schlager JJ. 2005. In vitro toxicity of nanoparticles in BRL 3A rat liver cells. Toxicol in Vitro 19:975–983.

Kaewamatawong T, Shimada A, Okajima M, Inoue H, Morita T, Inoue K, Takano H. 2006. Acute and subacute pulmonary toxicity of low dose of ultrafine colloidal silica particles in mice after intratracheal instillation. Toxicol Pathol 34:958.

Limbach LK, Wick P, Manser P, Grass RN, Bruinink A, Stark WJ. 2007. Exposure of engineered nanoparticles to human lung epithelial cells: Influence of chemical composition and catalytic activity on oxidative stress. Environ Sci Technol 41: 4158–4163.

Lok CN, Ho CM, Chen R, He QY, Yu WY, Sun HZ, Tam PKH, Chiu JF, Che CM. 2006. Proteomic analysis of the mode of antibacterial action of silver nanoparticles. J Proteome Res 5:916–924.

Lynch I, Dawson KA, Linse S. 2006. Detecting cryptic epitopes created by nanoparticles. Sci STKE 327:1–6.

Mosmann T. 1983. Rapid colorimetric assay for cellular growth and survival-application to proliferation and cytotoxicity assays. J Immunol Methods 65:55–63.

Nan AJ, Bai X, Son SJ, Lee SB, Ghandehari H. 2008. Cellular uptake and cytotoxicity of silica nanotubes. Nano Lett 8:2150–2154.

Navarro E, Piccapietra F, Wagner B, Marconi F, Kaegi R, Odzak N, Sigg L, Behra R. 2008. Toxicity of silver nanoparticles to Chlamydomonas reinhardtii. Environ Sci Technol 42: 8959–8964.

Nel A, Xia T, Madler L, Li N. 2006. Toxic potential of materials at the nanolevel. Science 311:622–627.

Nunez R. 2001. DNA measurement and cell cycle analysis by flow cytometry. Curr Issues Mol Biol 3:67–70.

Oberdörster G, Oberdörster E, Oberdörster J. 2005. Nanotoxicology: An emerging discipline evolving from studies of ultrafine particles. Environ Health Perspect 113:823–839.

Olcott CT. 1950. Experimental argyrosis. V. Hypertrophy of the left ventricule of the heart in rats ingesting silver salts. Arch Pathol 49:138–139.

Pan Y, Neuss S, Leifert A, Fischler M, Wen F, Simon U, Schmid G, Brandau W, Jahnen-Dechent W. 2007. Size-dependent cytotoxicity of gold nanoparticles. Small 3:1941–1949.

Service RF. 2003. Nanomaterials shows signs of toxicity. Science 300:243–243.

Shen J, Shan W, Zhang Y, Du J, Xu H, Fan K, Shen W, Tang Y. 2004. A novel catalyst with high activity for polyhydric alcohol oxidation: Nanosilver/zeolite film. Chem Commun 21: 2880–2881.

Susan WPW, Willie JGMP, Carla AH, Werner IH, Agnes GO, Evelyn HWH, Boris R, Julia B, Iise G, Dik VDM, Susan D, Wim HDJ, Maaike VZ, Adrienne JAMS, Robert EG. 2009. Nano-silver – a review of available data and knowledge gaps in human and environmental risk assessment. Nanotoxicology 3:109–138.

Takenaka S, Karg E, Roth C, Schulz H, Ziesenis A, Heinzmann U, Schramel P, Heyder J. 2001. Pulmonary and systemic distribution of inhaled ultrafine silver particles in rats. Environ Health Perspect 4(Suppl.):547–551.

Trop M, Novak M, Rodl S, Hellbom B, Kroell W, Goessler W. 2006. Silver-coated dressing Acticoat caused raised liver enzymes and argyria-like symptoms in burn patient. J Trauma 60:648–652.

Wang Y, Li D, Li P, Wang W, Ren W, Dong S, Wang E. 2007. Surface enhanced Raman scattering of brilliant green on AG nanoparticles and applications in living cells as optical probes. J Phys Chem C 111:16833–16839.

Zhang Y, Sun J. 2007. A Study on the bio-safety for nano-silver as anti-bacterial materials. Chin J Med Instrumen 31:35–38.